Paper AAS 02-101

Attitude Determination and Autonomous On-Orbit Calibration of Star Tracker For GIFTS Mission

Puneet Singla, D. Todd Griffith, J.L. Crassidis and J.L. Junkins

Department of Aerospace Engineering
Texas A&M University, College Station, TX 77843-3141

AAS/AIAA Space Flight Mechanics Meeting

San Antonio, Texas 27-30 January, 2002

AAS Publications Office, P.O. Box 28130, San Diego, CA 92129

ATTITUDE DETERMINATION AND AUTONOMOUS ON-ORBIT CALIBRATION OF STAR TRACKER FOR THE GIFTS MISSION

Puneet Singla,[1] D. Todd Griffith,[2] John L. Crassidis,[3] and John L. Junkins[4]

A novel split field of view star tracker is being developed for the EO-3 GIFTS mission (2004). The camera is designed to be autonomously self-calibrating, and capable of a rapid/reliable solution of the lost-in-space problem as well as recursive attitude estimation. Two efficient Kalman filter algorithms for attitude, camera principal point offset, and focal length estimation are developed. These algorithms make use of three axis gyros for the rate data and star camera split field-of-view line-of-sight vector measurements. To model the optics of the camera the pinhole model is used, which is found to be sufficiently accurate for most of star cameras. The relative merits of the two algorithms are then studied for estimating the principal point offset, focal length and attitude of a simulated spacecraft motion. Simulation results indicate that both algorithms produce precise attitude estimates by determining the principal point offset, focal length and rate bias; however, reliability and robustness characteristics favor the second algorithm.

Introduction

Spacecraft attitude determination is the process of estimating the orientation of a spacecraft by utilizing on-board observations of celestial bodies or other reference points. Combinations of these observations are used to generate more accurate estimates of the spacecraft rotational attitude. If these observations are error free then the spacecraft attitude can be determined precisely. But, in practical problems these measurements are not error free, so some sensor noise is always present. Several attitude sensors exist, including: three axis magnetometers, sun sensors, Earth-horizon sensors, global positioning sensors, star cameras, and rate integrating sensors. The accuracy of the attitude estimation depends on the quality of the attitude sensor. For example, the attitude accuracies that can be achieved with a sun sensor are approximately 0.015 degrees for the best available instruments.[1] For higher accuracies, star measurements are used as the key inputs for attitude estimation. Accuracies in the sub-arc second range are possible, but the drawbacks are the cost of star camera, complexity, and extensive software and calibration requirements. Systematic effects that require calibration are due to lens distortion and instrument aging. These systematic effects introduce error in the attitude estimate, and must be accounted for in order to achieve high-precision attitude determination. Ground based testing is used to calibrate the star cameras for these systematic errors, but this process requires the set up of high-precision laboratories. A novel algorithm for on-orbit autonomous calibration of star cameras is being developed for the EO-3 GIFTS mission to bring down the overall cost of the mission. This algorithm makes the overall system camera design adaptive to any possible sensor changes due to environment, aging electronics, and similar difficult-to-anticipate effects. Many algorithms are mentioned in the literature for the calibration of CCD array cameras;[2, 3] however, these are mainly for used laboratory calibration.

To improve the attitude estimation accuracy, the attitude is normally estimated by the combination of measurements of attitude along with the model of the spacecraft dynamics. The use of densely measured

[1]Graduate Student, 722 Bright Bldg., Department of Aerospace Engineering, Texas A&M University, College Station, TX 77843-3141, puneet@neo.tamu.edu
[2]Graduate Student, 722 Bright Bldg., Department of Aerospace Engineering, Texas A&M University, College Station, TX 77843-3141, dtg8332@aero.tamu.edu
[3]Assistant Professor, Department of Aerospace and Mechanical Engineering, University at Buffalo, State University of New York, Amherst, NY 14260-4400, Tel: (716) 645-2593, johnc@eng.buffalo.edu
[4]George J. Eppright Chair Professor, Director of the Center for Mechanics and Control, Department of Aerospace Engineering, Texas A&M University, College Station, TX 77843-3141, Tel: (979) 845-3912, Fax: (979) 845-6051, junkins@tamu.edu

rate data can omit the need for a dynamic model. But the rate sensors have inherent noise and systematic error problems, of which bias is the most important.

Attitude estimates must be calculated quickly and continuously during the entire operational life of the mission. During normal operations the problem is recursive, i.e., the attitude filter makes new predictions based on present and prior sensor information. The Kalman filter (Ref. 4,5,6,7,8) is one of the most widely used and powerful tools for real-time estimation problems. The Kalman filter minimizes the trace of the covariance of the estimate error between the model response and actual measurements in the least squares sense. The main advantage of a Kalman filter over other methods for attitude estimation is that it combines the rate data measurements with the attitude sensor data to give more accurate estimates than using each sensor alone. Optimal filter design depends upon the properties of the measurement and process noise (in this case the process noise is a function of the gyro model parameters).

In this paper we will present attitude determination results using the Extended Kalman filter for both single field-of-view (FOV) and dual field-of-view cameras. A modified version of the algorithm for interlock angle estimation is also presented. Two efficient recursive algorithms will be discussed for boresight and focal plane calibration. Both attitude dependent and attitude independent methods for the calibration problem are given. The relative merits of the two algorithms are then studied for star camera calibration and attitude determination. Reliability and robustness characteristics favor the attitude independent algorithm.

Attitude Kinematics

Spacecraft attitude can be represented by various parameters, for example Euler angles, Rodrigues parameters, modified Rodrigues parameters and quaternions or Euler parameters. Quaternions are ideal and the most widely used parameterization for attitude estimation for the following reasons (Ref. 1,4,5,9,10):

1. The attitude matrix is algebraic in nature.
2. The parameterization is free from singularities.
3. The kinematic equations are linear in nature.

Generally, elements of the quaternions are expressed in terms of the principal eigenvector **e** and rotation α about the **e** as follows (Ref. 1,5,6):

$$\begin{aligned} q_1 &= e_1 \sin(\alpha/2) \\ q_2 &= e_2 \sin(\alpha/2) \\ q_3 &= e_3 \sin(\alpha/2) \\ q_4 &= \cos(\alpha/2) \end{aligned} \tag{1}$$

Clearly, the elements of the quaternion satisfy a unit norm constraint. The direction cosine matrix can be expressed in terms of the quaternions as (Ref. 1,5,10):

$$\left[\mathbf{C}(\mathbf{q})\right] = \left(q_4^2 - \mathbf{q}^T\mathbf{q}\right)\mathbf{I}_{3\times 3} + 2\mathbf{q}\mathbf{q}^T - 2q_4[\mathbf{q}\otimes] \tag{2}$$

Where,

$$[\mathbf{q}\otimes] = \begin{bmatrix} 0 & -q_3 & q_2 \\ q_3 & 0 & -q_1 \\ -q_2 & q_1 & 0 \end{bmatrix} \tag{3}$$

A successive composition in terms of quaternions is performed by quaternion multiplication (Ref. 1,5,10). The result of the multiplication of two quaternions is a third quaternion, which yields the same direction cosine matrix given by the multiplication of the corresponding direction cosine matrices:

$$\begin{aligned} [\mathbf{C}(\mathbf{q}'')] &= [\mathbf{C}(\mathbf{q}')][\mathbf{C}(\mathbf{q})] \\ &\Updownarrow \\ \mathbf{q}'' &= \mathbf{q}'\otimes\mathbf{q} = [\mathbf{q}']\mathbf{q} \end{aligned} \tag{4}$$

where,

$$[q'] = \begin{bmatrix} q_4' & q_3' & -q_2' & q_1' \\ -q_3' & q_4' & q_1' & q_2' \\ q_2' & -q_1' & q_4' & q_3' \\ -q_1' & -q_2' & -q_3' & q_4' \end{bmatrix} \tag{5}$$

The spacecraft kinematic equations of motion in terms of quaternions can be derived by taking the time derivative of equation (2) (Ref. 1,5,10):

$$\dot{\mathbf{q}}(t) = \frac{1}{2}\boldsymbol{\Omega}\left(\boldsymbol{\omega}(t)\right)\mathbf{q}(t) = \frac{1}{2}\boldsymbol{\Xi}\left(\mathbf{q}(t)\right)\boldsymbol{\omega}(t) \tag{6}$$

where, $\boldsymbol{\Omega}(\boldsymbol{\omega})$ and $\boldsymbol{\Xi}(\mathbf{q})$ are defined as,

$$\boldsymbol{\Omega}(\boldsymbol{\omega}) \equiv \begin{bmatrix} [-\boldsymbol{\omega}\otimes] & \vdots & \boldsymbol{\omega} \\ -\boldsymbol{\omega}^T & \vdots & 0 \end{bmatrix}, \quad \boldsymbol{\Xi}(\mathbf{q}) \equiv \begin{bmatrix} q_4\mathbf{I}_{3\times 3} + [\mathbf{q}\times] \\ -\mathbf{q}^T \end{bmatrix} \tag{7}$$

Kalman Filter Formulation

The Kalman filter is the most widely used sequential estimator for the spacecraft attitude determination problem. The Kalman filter minimizes the trace of the covariance of the estimate error between the model response and the actual measurements in the least squares sense, but due to its recursive structure, it is computationally more efficient than the batch least squares algorithm, where a large set of measurement data has to be processed simultaneously. The main advantage of the Kalman filter for attitude determination is that it optimally combines the rate data with the attitude sensor data to produce more accurate results. The Extended Kalman filter (EKF) for non-linear systems uses the linearized state-space model about the current estimate of the states to generate the update at a measurement time, and propagates the estimates between the measurement times. There are many excellent sources on this subject, and the derivation of EKF equations can be found in (Ref. 5,6,8,10). The EKF equations can be divided into two categories: Prediction and Update equations. The Prediction part of the EKF requires a model for the dynamics of the system, while the update part requires a measurement model. A summary of the EKF equations is given below.

Dynamic Model: $\dot{\vec{\mathbf{x}}} = \mathbf{f}\left(\vec{\mathbf{x}}(t), t\right) + \mathbf{G}\left(\vec{\mathbf{x}}(t), t\right)\mathbf{w}(t)$ (8)

Measurement Model: $\mathbf{Y} = \mathbf{h}(\mathbf{x}(t)) + \boldsymbol{\upsilon}$ (9)

With,

$$E\left[\mathbf{w}(t)\right] = 0 \;\&\; E\left[\mathbf{w}(t)\mathbf{w}^T(t')\right] = \mathbf{Q}(t)\delta\left(t - t'\right)$$

$$\Delta\mathbf{x}(t) = \mathbf{x}(t) - \hat{\mathbf{x}}(t) \;\&\; \mathbf{P}(t) = \mathbf{E}[\Delta\mathbf{x}(t)\Delta\mathbf{x}^{\mathbf{T}}(t)]$$

$$E\left[\boldsymbol{\upsilon}(t)\right] = 0 \;\&\; E\left[\boldsymbol{\upsilon}(t)\boldsymbol{\upsilon}^T(t')\right] = \mathbf{R}(t)\delta\left(t - t'\right)$$

Propagation:

$$\Delta\mathbf{x}(t) = \mathbf{F}(t)\Delta\mathbf{x}(t) + \mathbf{G}(t)\mathbf{w}(t)$$

$$\dot{\mathbf{P}} = \hat{\mathbf{F}}\mathbf{P} + \mathbf{P}^{\mathbf{T}}\hat{\mathbf{F}} + \hat{\mathbf{G}}\mathbf{Q}\hat{\mathbf{G}}^{\mathbf{T}} \tag{10}$$

where,

$$\mathbf{F}(t) = \frac{\partial}{\partial\mathbf{x}}\mathbf{f}(\mathbf{x}, t)_{\hat{x}(t)}$$

Update:

$$\hat{\mathbf{x}}_k(+) = \hat{\mathbf{x}}_k(-) + \mathbf{K}_k\left[\mathbf{Y}_k - \mathbf{h}_k\left(\hat{\mathbf{x}}_k(-)\right)\right]$$

$$\mathbf{P}_k(+) = \left[\mathbf{I} - \mathbf{K}_k\mathbf{H}_k\left(\hat{\mathbf{x}}_k(-)\right)\right]\mathbf{P}_k(-) \tag{11}$$

$$\mathbf{K}_k = \mathbf{P}_k(-)\mathbf{H}_k^T\left[\mathbf{H}_k\mathbf{P}_k(-)\mathbf{H}_k^T + \mathbf{R}\right]^{-1}$$

The above equations are formulated by assuming the process and measurement noise to be Gaussian white noise; further it is also assumed that the sensitivity matrix **H** is free of any kind of error. Optimal filter design depends upon the tuning and the properties of measurement and process noise. To use the Kalman filter, we have to first identify our measurement and dynamical model.

Measurement Model

A Dual Field of view star tracker will be used as the attitude sensor for the EO-3 GIFTS mission. Star positions are the most accurate source of reference celestial bodies for the attitude determination, as their position with respect to an inertial frame is fixed. Spacecraft attitude is determined by taking the photographs of the stars by using a CCD camera. Pixel formats of the order of 512×512 or larger are commonly used to provide good resolution pictures. The first stage in attitude determination is to identify a star with reference to an on-board star catalog. After star identification is made,[12,13] image plane coordinates of the stars are given by using a pinhole camera model for the camera (Ref. 2,5). Photograph image plane coordinates of j^{th} star are given by following co-linearity equations:

$$x_j = x_o - f\frac{(C_{11}r_{x_j} + C_{12}r_{y_j} + C_{13}r_{z_j})}{(C_{13}r_{x_j} + C_{32}r_{y_j} + C_{33}r_{z_j})}$$
$$y_j = y_o - f\frac{(C_{21}r_{x_j} + C_{22}r_{y_j} + C_{23}r_{z_j})}{(C_{13}r_{x_j} + C_{32}r_{y_j} + C_{33}r_{z_j})} \tag{12}$$

where f is the camera focal length determined by ground or on-orbit calibration, C_{ij} are the direction cosine matrix elements, and the inertial star vector $\mathbf{r_j}$ is given by

$$\mathbf{r}_j = \begin{Bmatrix} r_{x_j} \\ r_{y_j} \\ r_{z_j} \end{Bmatrix} = \begin{Bmatrix} \cos\delta_j \cos\alpha_j \\ \cos\delta_j \sin\alpha_j \\ \sin\delta_j \end{Bmatrix} \tag{13}$$

Choosing the z-axis of the image coordinate system towards the boresight of the camera as shown in figure 1, and measurement unit vector $\mathbf{b_j}$ is given by following equation:

$$\mathbf{b}_j = \frac{1}{\sqrt{x_j^2 + y_j^2 + f^2}} \begin{bmatrix} -x_j \\ -y_j \\ f \end{bmatrix} \tag{14}$$

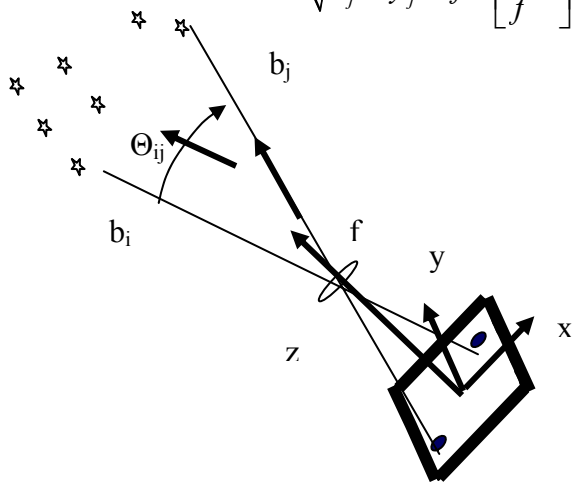

Figure 1: Star Positions in the Image Space

The relation between measured star direction vectors $\mathbf{b}_j$ in image space and their projection $\mathbf{r}_j$ on the inertial frame is given by

$$\mathbf{b}_j = \mathbf{C}\,\mathbf{r}_j + \boldsymbol{\upsilon}_j \tag{15}$$

where $\boldsymbol{\upsilon}_j$ is a zero mean Gaussian white-noise process with covariance $\mathbf{R}_j$. Therefore the attitude determination problem reduces to the estimation of the different elements of the attitude matrix **C**, which can be parameterized in terms of the quaternion as given in equation (2).

Gyro Model

Rate gyros are used to measure the angular rates of the spacecraft without regard to the attitude of the spacecraft. Rate gyros provide the angular rates of the spacecraft to a very high accuracy. With rate data, the well-known kinematics model of spacecraft can replace the dynamical model. But the rate sensors have their own inherent noise problems, where the noise level of the sensor and bias (constant drift) are the two main characteristics of the rate data. Bias estimation is very important for attitude determination using rate data. The gyro model is given by (Ref.4,5,10,11)

$$\boldsymbol{\omega} = \tilde{\boldsymbol{\omega}} - \mathbf{b} - \boldsymbol{\eta}_1 \tag{16}$$

where $\boldsymbol{\omega}$ is the true angular velocity, $\tilde{\boldsymbol{\omega}}$ is the gyro measured angular velocity, and **b** is the gyro bias vector, which is further modeled by

$$\dot{\mathbf{b}} = \boldsymbol{\eta}_2 \tag{17}$$

where η_1 and η_2 are assumed to be modeled by a Gaussian white-noise process with standard deviation of σ_u and σ_v. Defining the noise vector:

$$\mathbf{w} = \begin{bmatrix} \eta_1 \\ \eta_2 \end{bmatrix} \tag{18}$$

then the statistical properties are assumed to be known as

$$E\left[\mathbf{w}(t)\right] = 0 \;\&\; E\left[\mathbf{w}(t)\mathbf{w}^T(t')\right] = \mathbf{Q}(t)\delta\left(t - t'\right) \tag{19}$$

Here, **Q** is computed to be[11]

$$\mathbf{Q} = \begin{bmatrix} \sigma_v^2 T + 1/3\,\sigma_u^2 T^3 & -1/2\sigma_u^2 T^2 \\ -1/2\sigma_u^2 T^2 & \sigma_u^2 T \end{bmatrix} \tag{20}$$

and T is the sampling time of gyro data.

EKF Formulation For Quaternion Parameterization

The redundancy of the four-parameter description of the quaternion generates a singularity in the covariance matrix **P** of the Kalman filter. Define

$$\Delta\mathbf{q} = \mathbf{q} - \hat{\mathbf{q}}$$

Assuming that the estimated quaternion is close to the true quaternion, then

$$\begin{aligned} \Delta\mathbf{q}^T\hat{\mathbf{q}} &\simeq 0 \\ \mathbf{P}\hat{\mathbf{q}} &= E\left[\Delta\mathbf{q}\left(\Delta\mathbf{q}^T\hat{\mathbf{q}}\right)\right] = 0 \end{aligned} \tag{21}$$

Hence, **q** lies in the null space of **P**, which generates a singularity in the covariance matrix **P**. Lefferts, Markley and Shuster[10] have proposed three methods to take into account the singularity in covariance matrix:

1. Reduced representation of the covariance matrix.
2. The truncated covariance representation.
3. The body fixed covariance representation.

In this paper the Extended Kalman filter formulation is based upon the third approach. In this approach, an error quaternion is defined, which is the composition of the true quaternion and inverse estimated quaternion:

$$\delta\mathbf{q} = \mathbf{q} \otimes \hat{\mathbf{q}}^{-1} \tag{22}$$

From equations (4), (7) and (22), we can show that

$$\delta\mathbf{q} = \mathbf{\Xi}^T(\hat{\mathbf{q}})\mathbf{q} \text{ and } \delta q_4 = \hat{\mathbf{q}}^T\mathbf{q} \approx 1 \tag{23}$$

Since the fourth component of error quaternion is close to unity, only the vector part of error quaternion is of interest to us. So the state vector for the EKF consists of only the 3×1 vector part of error quaternion and the 3×1 vector of gyro biases.

$$\mathbf{x} = \begin{bmatrix} \delta\mathbf{q} \\ \mathbf{b} \end{bmatrix} \tag{24}$$

The state equations for new state vector using the gyro model, given in equations (16) and (17), are given by[10]

$$\delta\dot{\mathbf{q}} = -\hat{\boldsymbol{\omega}} \times \delta\mathbf{q} - 1/2\left(\Delta\mathbf{b} + \boldsymbol{\eta}_1\right) \text{ and } \delta\dot{q}_4 = \Delta\dot{\mathbf{b}} = \mathbf{0} \tag{25}$$

where

$$\hat{\boldsymbol{\omega}} = \tilde{\boldsymbol{\omega}} - \hat{\mathbf{b}} \tag{26}$$

So the **F** and **G** matrices in equation (10) are given by

$$\mathbf{F} = \begin{bmatrix} -[\hat{\boldsymbol{\omega}} \otimes] & -1/2\,\mathbf{I}_{3\times3} \\ \mathbf{O}_{3\times3} & \mathbf{I}_{3\times3} \end{bmatrix}, \quad \mathbf{G} = \begin{bmatrix} -1/2\,\mathbf{I}_{3\times3} & \mathbf{O}_{3\times3} \\ \mathbf{O}_{3\times3} & \mathbf{I}_{3\times3} \end{bmatrix} \tag{27}$$

From equation (25), the quaternion prediction equation is given by

$$\begin{aligned} \hat{\mathbf{q}}_k &= [\cos(\theta_{k-1}/2)\mathbf{I}_{4\times4} + \sin(\theta_{k-1}/2)\mathbf{\Omega}(\hat{\mathbf{e}}_{k-1})]\hat{\mathbf{q}}_{k-1} \\ \theta_{k-1} &= \hat{\boldsymbol{\omega}}_{k-1}\left(t_k - t_{k-1}\right) \end{aligned} \tag{28}$$

and the covariance prediction is given by

$$\begin{aligned} &\mathbf{P}_k = \mathbf{\Phi}_{k-1}\mathbf{P}_{k-1}\mathbf{\Phi}_{k-1} + \mathbf{G}\mathbf{Q}_{k-1}\mathbf{G}, \ \mathbf{\Phi}_{k-1} = \begin{bmatrix} \mathbf{\Phi}_1 & \mathbf{\Phi}_2 \\ \mathbf{O}_{3\times3} & \mathbf{I}_{3\times3} \end{bmatrix} \\ &\mathbf{\Phi}_1 = \mathbf{I}_{3\times3} + [\boldsymbol{\omega} \otimes]^T / \left(\boldsymbol{\omega}^T\boldsymbol{\omega}\right)^{1/2} \sin(\theta_{k-1}) + \left([\boldsymbol{\omega} \otimes]^T / \left(\boldsymbol{\omega}^T\boldsymbol{\omega}\right)^{1/2}\right)^2 \left(1 - \cos(\theta_{k-1})\right) \\ &\mathbf{\Phi}_2 = \left(\mathbf{I}_{3\times3}\Delta t + [\boldsymbol{\omega} \otimes]^T \left(1 - \cos(\theta_{k-1})\right)\right) / \left(\boldsymbol{\omega}^T\boldsymbol{\omega}\right) + [\boldsymbol{\omega} \otimes][\boldsymbol{\omega} \otimes]\left(\theta_{k-1} - \sin(\theta_{k-1})\right) / \left(\boldsymbol{\omega}^T\boldsymbol{\omega}\right)^{3/2} \end{aligned} \tag{29}$$

According to equations (11) and (15), the sensitivity matrix **H** is given by

$$\mathbf{H} = [\mathbf{L} \ \ \mathbf{O}_{3\times3}] \tag{30}$$

where

$$\mathbf{L} = \frac{\partial(\mathbf{b})}{\partial(\delta\mathbf{q})} = \frac{\partial\left(\mathbf{C}(\mathbf{q})\mathbf{r}\right)}{\partial(\delta\mathbf{q})} \tag{31}$$

According to the definition of error quaternion:

$$\mathbf{C}(\mathbf{q}) = \mathbf{C}(\delta\mathbf{q})\mathbf{C}(\hat{\mathbf{q}}) \tag{32}$$

From equation (2), we can show that the differential **δq** update results in

$$\mathbf{C}(\delta\mathbf{q}) \approx \mathbf{I}_{3\times3} - 2[\boldsymbol{\delta}\mathbf{q}\otimes] \approx \mathbf{I}_{3\times3} - [\boldsymbol{\delta}\boldsymbol{\alpha}\otimes] \tag{33}$$

where **δq** is the error quaternion and **δα** is the small angle approximation. Substituting equation (33) into (32) and further substituting equation (32) into (31) gives

$$\mathbf{L} = 2[\hat{\mathbf{b}}\otimes] = 2[(\mathbf{C}(\hat{\mathbf{q}})\mathbf{r})\otimes] \tag{34}$$

Simulations

The design specifications for the EO-3 GIFTS mission require rate data to be sampled at 200Hz and star data at 10Hz. Figure 2 describes the data flow between different software modules for the GIFTS mission (CM in figure 2 denotes the GIFTS control module), while figure 3 describes the main parts of Kalman filter algorithm for attitude determination. The prediction loop of the Kalman filter depends upon the rate data frequency, while update frequency depends upon image processing, centroiding, star identification and star-tracker data frequencies.

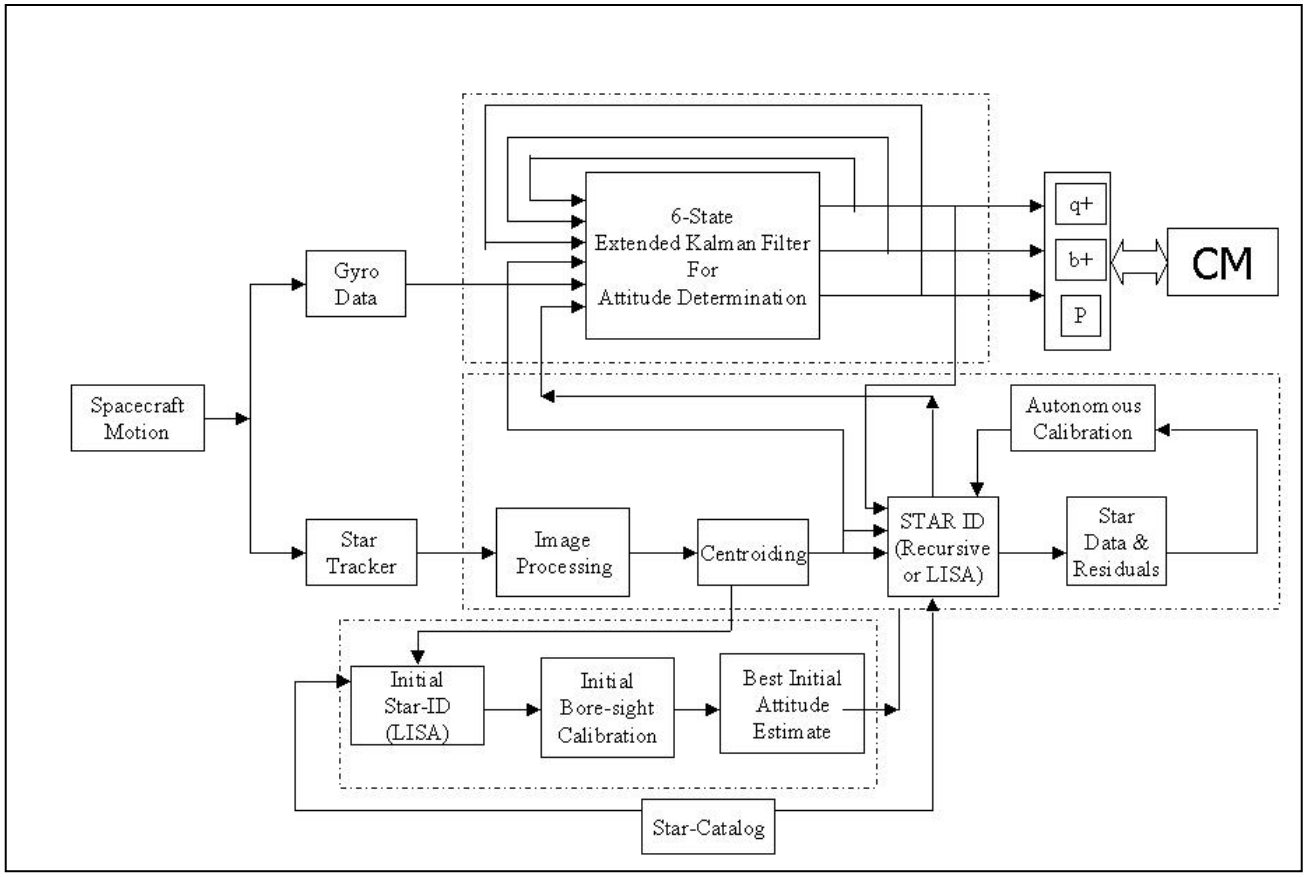

Figure 2: Macroscopic Data Flow for GIFTS Mission

Using the J-2000 star catalog with stars of magnitude up to 6.4, assuming $8^{\circ}\times8^{\circ}$ field of view star camera and 17μ radian (for 1024×1024 pixel array) of centroiding error, star data are simulated. Simulations are done for single FOV. Plots of attitude error and estimated gyro bias for single FOV star cameras are shown in figures 4 and 5, respectively. As the z-axis of image coordinate system coincides with the bore-sight axis of the camera, less information is available for the rotation about the z-axis, which corresponds to higher covariance in the yaw angle estimates. The same fact can be verified by the singular value decomposition (SVD) of the observability matrix. Singular values of the observability matrix give us an idea about the degree of observability of the states and the columns of **V** show the degree of cross

correlated observability of states. The singular values and columns of the observability matrix $\mathbf{O}=[\mathbf{H}^T (\mathbf{HF})^T (\mathbf{HF}^2)^T (\mathbf{HF}^3)^T (\mathbf{HF}^4)^T (\mathbf{HF}^5)^T]^T$ are given below:

$$\mathbf{S} = \begin{bmatrix} 2.0 \\ 2.0 \\ 1.0 \\ 0.99 \\ 2.3\text{e-}2 \\ 4.7\text{e-}17 \end{bmatrix}, \quad \mathbf{V} = \begin{bmatrix} -9.9818\text{e-}001 & 4.3523\text{e-}002 & -9.8640\text{e-}004 & -1.7468\text{e-}002 & 6.0839\text{e-}006 & 3.7986\text{e-}002 \\ 5.7768\text{e-}002 & 7.5097\text{e-}001 & -1.7119\text{e-}002 & 1.0109\text{e-}003 & -3.5210\text{e-}007 & 6.5758\text{e-}001 \\ -9.3680\text{e-}005 & -6.5867\text{e-}001 & -4.6119\text{e-}002 & -1.6394\text{e-}006 & 5.7098\text{e-}010 & 7.5102\text{e-}001 \\ -7.6173\text{e-}004 & -1.7471\text{e-}002 & 9.9712\text{e-}001 & 4.3515\text{e-}002 & -3.8000\text{e-}002 & 4.5910\text{e-}002 \\ -1.3143\text{e-}002 & 1.0111\text{e-}003 & -5.7707\text{e-}002 & 7.5084\text{e-}001 & -6.5783\text{e-}001 & -2.6570\text{e-}003 \\ 1.1524\text{e-}002 & -1.6397\text{e-}006 & 9.3581\text{e-}005 & -6.5882\text{e-}001 & -7.5221\text{e-}001 & 4.3087\text{e-}006 \end{bmatrix} \tag{35}$$

The sixth column of the **V** corresponds to the zero singular value and shows that the yaw angle state is poorly observable. Thus the covariance related to yaw angle state is higher than the covariance of the pitch and roll angle states.

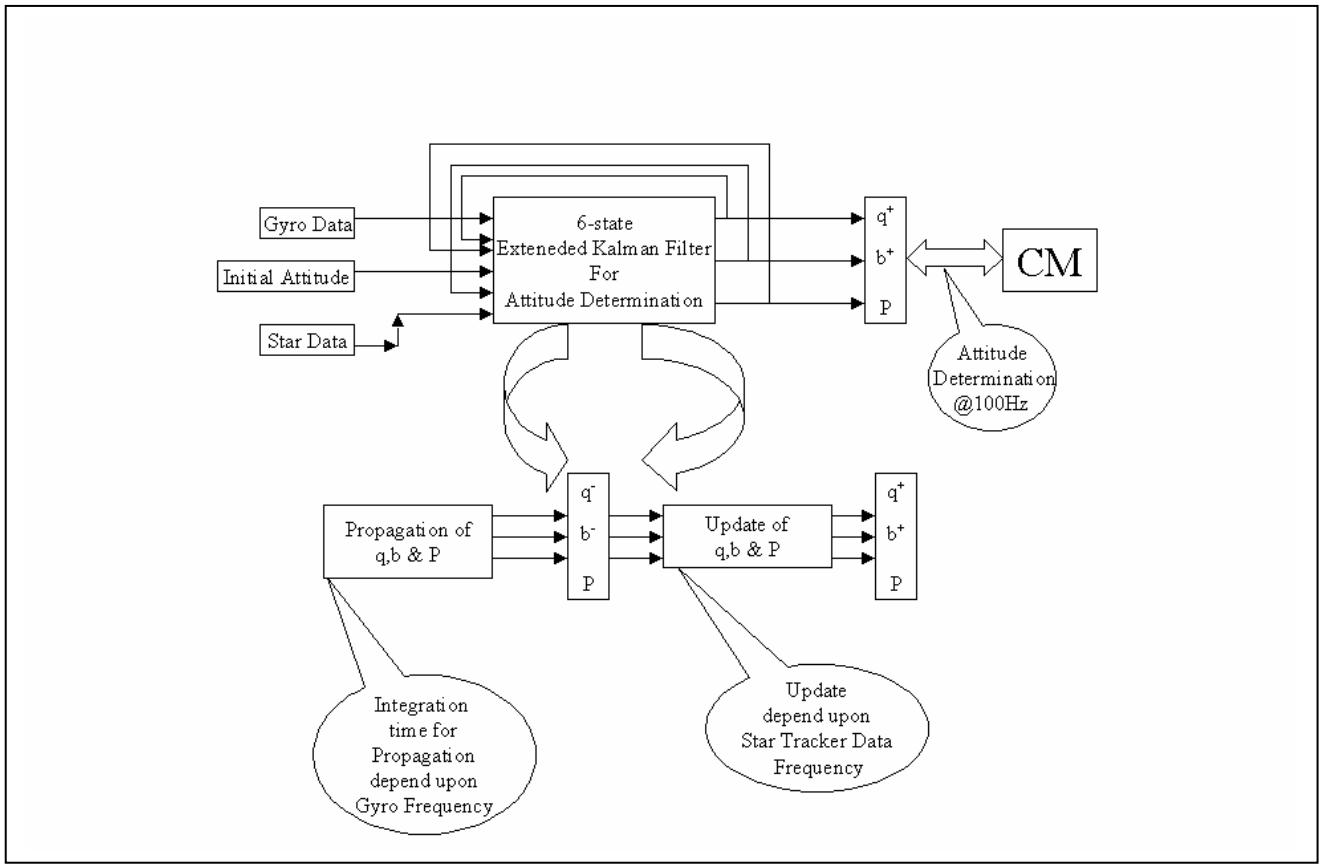

Figure 3: Extended Kalman Filter Flow Chart

Figures 6 and 7 show the plots of attitude error and estimated gyro bias, respectively, for the dual FOV camera. In this case the z-axis of image plane coordinate system coincides with the boresight axis of one FOV, but information of the rotation about the z-axis is available from the other FOV (perpendicular to first one). So the dual FOV star camera gives a more accurate attitude estimate than the single FOV case. It is clear from the results that attitude accuracy estimates of 5μrad about each axis can be obtained for a dual FOV star camera.

The accuracy of the results implicitly depends on the knowledge of the interlock angle between the two FOVs, as stars from both FOVs are projected on same focal plane detector (say FOV-A). The interlock uncertainty is not accounted for above, therefore the estimation of interlock angle between two FOV is very important. Figure 8 shows a flow chart for an algorithm to estimate the interlock angle between the two FOVs. The state vector of the EKF is now appended with three extra states corresponding to an error quaternion for FOV-B. Basically, the new Kalman filter is the combination of two Kalman filters working in tandem with each other. For simulation purposes, star-data in two perpendicular FOVs are generated and then data from the second FOV-B is projected onto the FOV-A detector and used as measurements for the Kalman filter. Using the current estimate of the interlock angle, stars from FOV-B, identified in FOV-A are projected back into FOV-B and used as measurements for the attitude estimation of FOV-B. Figures 9, 10 and 11 show the attitude errors for FOV-A and FOV-B and bias estimates, respectively. From these plots, it is clear that the EKF algorithm developed in this paper is able to estimate the attitude, interlock angle and gyro bias accurately.

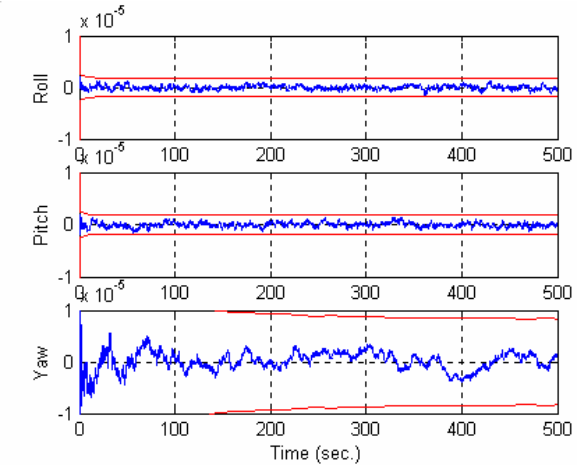

Figure:4: Attitude Errors and 3σ Bounds

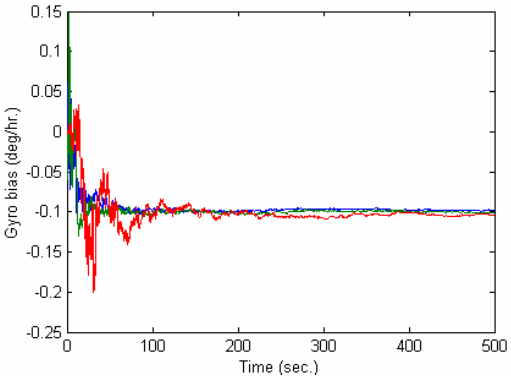

Figure 5: Estimated Gyro Biases

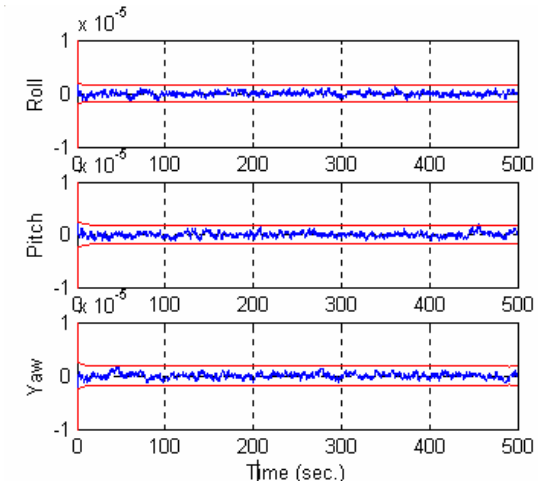

Figure 6: Attitude Errors and 3σ Bounds
for Dual Field-of-View Star Camera

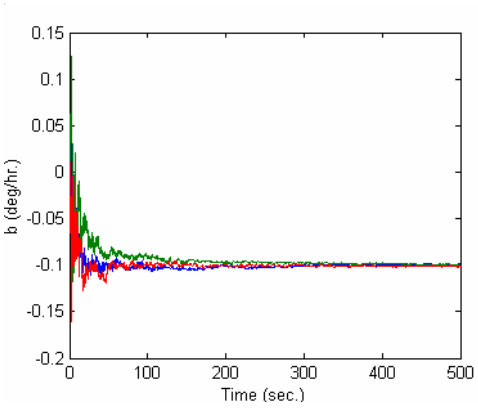

Figure 7: Estimated Gyro Biases

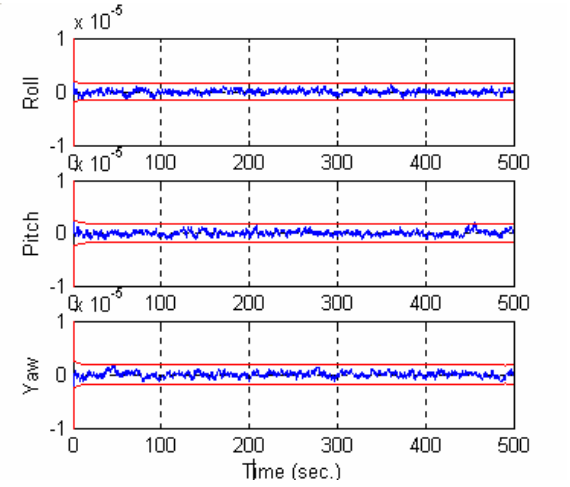

Figure 9: Attitude Errors and 3σ Bounds for FOV-A of Dual Field-of-View Star Camera

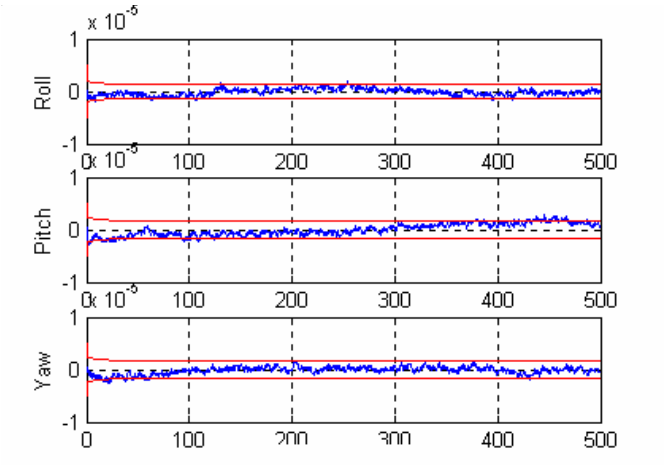

Figure 10: Attitude Errors and 3σ Bounds for FOV-B of Dual Field-of-view Star Camera

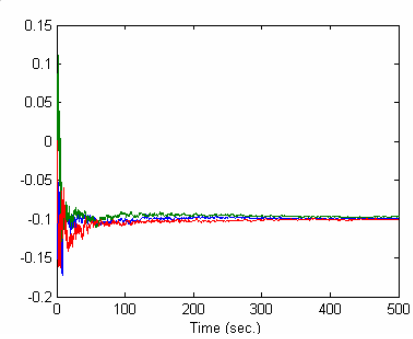

Figure 11: Estimated Rate Biases

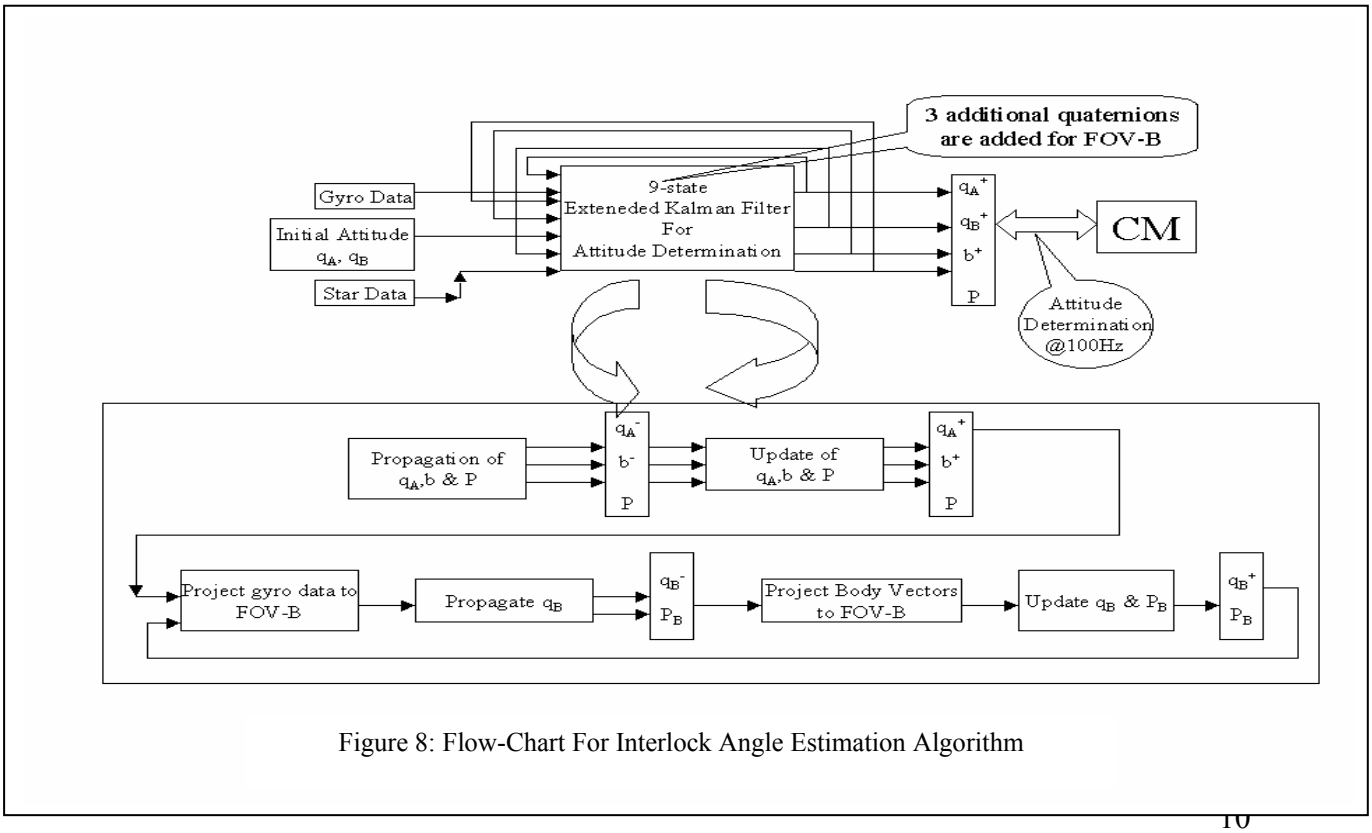

Figure 8: Flow-Chart For Interlock Angle Estimation Algorithm

Covariance Analysis

A residual covariance analysis can be used to check the consistency of the attitude errors. According to equations (32) and (33), the estimated and true attitude are related as

$$\mathbf{C}(\mathbf{q}) = \mathbf{C}(\boldsymbol{\delta q})\mathbf{C}(\mathbf{q}) \approx (\mathbf{I} - [\boldsymbol{\delta\alpha}\otimes])\mathbf{C}(\mathbf{q}) \tag{35}$$

Substituting equation (35) into equation (15) gives

$$\tilde{\mathbf{b}}_\mathbf{i} = (\mathbf{I} - [\boldsymbol{\delta\alpha}\otimes])\mathbf{C}(\hat{\mathbf{q}})\mathbf{r}_i = \mathbf{C}(\hat{\mathbf{q}})\mathbf{r}_i + [\mathbf{C}(\hat{\mathbf{q}})\mathbf{r}_i\otimes]\boldsymbol{\delta\alpha} \tag{36}$$

Therefore, the residual is given by

$$\tilde{\mathbf{b}}_i - \hat{\mathbf{b}}_i = \boldsymbol{\nu}_i - [\mathbf{C}(\hat{\mathbf{q}})\mathbf{r}_i\otimes]\boldsymbol{\delta\alpha} \tag{37}$$

We now need to determine a relationship between the attitude error and the measurement noise using the computed attitude. This is accomplished by directly using Wahba's loss function:[14]

$$\mathbf{J} = \frac{1}{2}\sum_{i=1}^{n}\left(\tilde{\mathbf{b}}_i - \hat{\mathbf{b}}_i\right)^T \mathbf{R}_i^{-1}\left(\tilde{\mathbf{b}}_i - \hat{\mathbf{b}}_i\right) \tag{38}$$

where n is the total number of vector measurements. Substituting equation (37) into equation (38), taking the partial with respect to $\boldsymbol{\delta\alpha}$ and setting the resultant to zero leads to

$$\boldsymbol{\delta\alpha} = \left(\mathbf{H}^T\mathbf{R}^{-1}\mathbf{H}\right)^{-1}\mathbf{H}^T\mathbf{R}^{-1}\boldsymbol{\nu} \tag{39}$$

where

$$\mathbf{H} = \begin{bmatrix} [\mathbf{C}(\mathbf{q})\mathbf{r}_1\otimes] \\ [\mathbf{C}(\mathbf{q})\mathbf{r}_2\otimes] \\ . \\ . \\ . \\ [\mathbf{C}(\mathbf{q})\mathbf{r}_n\otimes] \end{bmatrix}, \mathbf{R} = \begin{bmatrix} \mathbf{R}_1 & 0 & . & . & . & 0 \\ 0 & \mathbf{R}_2 & . & . & . & 0 \\ . & . & . & & & . \\ . & . & & . & & . \\ . & . & & & . & . \\ 0 & 0 & . & . & . & \mathbf{R}_n \end{bmatrix}, \nu = \begin{bmatrix} \boldsymbol{\nu}_1 \\ \boldsymbol{\nu}_2 \\ . \\ . \\ . \\ \boldsymbol{\nu}_n \end{bmatrix} \tag{40}$$

We recognize that $\mathbf{P}\equiv(\mathbf{H}^T\mathbf{R}^{-1}\mathbf{H})^{-1}$ is the attitude error covariance derived from a least squares formulation. Next, since the vector measurements errors are uncorrelated we have

$$E\left\{\left(\mathbf{H}^T\mathbf{R}^{-1}\mathbf{H}\right)^{-1}\mathbf{H}^T\mathbf{R}^{-1}\boldsymbol{\nu}\boldsymbol{\nu}_i^T\right\} = \left(\mathbf{H}^T\mathbf{R}^{-1}\mathbf{H}\right)^{-1}\left[\mathbf{C}(\mathbf{q})\mathbf{r}_i\otimes\right]^T \equiv P\left[\mathbf{C}(\mathbf{q})\mathbf{r}_i\otimes\right]^T \tag{41}$$

Therefore, substituting equation (39) into equation (37) and using the relationship in equation (41) leads to

$$\boldsymbol{\gamma}_i \equiv E\left\{\left(\tilde{\mathbf{b}}_i - \hat{\mathbf{b}}_i\right)\left(\tilde{\mathbf{b}}_i - \hat{\mathbf{b}}_i\right)^T\right\} = \mathbf{R}_i - \left[\mathbf{C}(\mathbf{q})\mathbf{r}_i\otimes\right]\mathbf{P}\left[\mathbf{C}(\mathbf{q})\mathbf{r}_i\otimes\right]^T \tag{42}$$

The right hand-side of the equation (42) can be computed independently of the attitude using equation (15), and the left hand-side is numerically computed. The matrix $\boldsymbol{\gamma}_\mathbf{i}$ is computed recursively by

$$\boldsymbol{\gamma}_i(k+1) = \boldsymbol{\gamma}_i(k) + \frac{1}{k+1}\left\{\frac{k}{k+1}\left[\mathbf{e}_i(k+1) - \overline{\mathbf{e}}_i(k)\right]\left[\mathbf{e}_i(k+1) - \overline{\mathbf{e}}_i(k)\right]^T - \boldsymbol{\gamma}_i(k)\right\} \quad (43)$$

$$\overline{\mathbf{e}}_i(k+1) = \overline{\mathbf{e}}_i(k) + \frac{1}{k+1}\left[\mathbf{e}_i(k+1) - \overline{\mathbf{e}}_i(k)\right]$$

where $\mathbf{e}_i \equiv \tilde{\mathbf{b}}_i - \hat{\mathbf{b}}_i$ and $\overline{\mathbf{e}}_i$ is the mean. Equation (42) is used to check the validity of the attitude determination algorithm. From simulation results, it is found that $\boldsymbol{\gamma}_i \leq R_i$, i.e., the error covariance is inline with the projected random error magnitude, and the left hand-side of the equation (42) matches well with the right hand-side.

CCD Camera Calibration

Star camera calibration is an important task in attitude determination of the spacecraft using the star trackers as attitude data sensors. The accuracy of attitude estimation depends upon the calibration of the star camera. The design specification for GIFTS attitude accuracy is 5 μrad. Therefore, for this mission the accuracy for attitude determination will require a well-calibrated star camera. Generally, star cameras are calibrated on the ground in very high precision laboratories. However, any significant change in the instrument or the environment can result in this calibration being inaccurate on-orbit. Therefore, the precise nature of the systematic errors for the star camera system should be and will be determined on-orbit, and the proper corrections will be applied on-orbit. A key question regarding the proper selection of a calibration approach is "How irregular is the distortion?" A global best fit of distortions should be sufficient if the slope of the distortion map is smooth globally. In the presence of localized distortions, a more judicious selection of the calibration approach will be required. In this section, several approaches for on-orbit calibration of star tracker camera for the EO-3 GIFTS mission (2004) are discussed. These approaches are quite general in nature and show promise for many future on-orbit calibration requirements. The calibration process is mainly divided into two major parts:

1. Calibration of principal point offset (x_0, y_0) and focal length (f).
2. Calibration of focal plane image distortions due to all other effects (lens distortions, misalignment, detector alignment, etc.).[15]

Generally, the implicit pinhole camera model is not exact so we need to find the best effective estimates of principal point offset (x_0, y_0) and focal length (f). In this paper, calibration of principal point offset and focal length is discussed in detail. Two approaches have been developed for the recursive estimation of principal point offset error and focal length.

Attitude Dependent Approach

In the first approach, the boresight error and focal length are determined by projecting the inertial catalogued star vectors into body frame using the best estimated attitude. But the problem with this approach is that the attitude itself depends upon the estimate of boresight error and focal length. A nested Kalman filter with the gyro bias and attitude being estimated in one filter and the principal point offset and effective focal length in other using the pinhole camera model is developed. The nested Kalman filter is needed, since the principal point offset and focal length are very weakly observable with spacecraft attitude and rate bias. The singular values and corresponding **V** matrix of observability matrix are given by

$$\mathbf{S} = \begin{bmatrix} 6.3223 & 6.3207 & 3.1610 & 3.1602 & 0.2908 & 0.1452 & 0.1062 & 0.00017 & 0.0001 \end{bmatrix}^T$$

$$\mathbf{V} = \begin{bmatrix} -0.8952 & -0.4451 & 0.0003 & 0.0006 & -0.0206 & 0.0000 & 0.0057 & 0.0001 & 0.0082 \\ -0.4450 & 0.8954 & -0.0007 & 0.0003 & -0.0093 & -0.0000 & 0.0005 & -0.0002 & 0.0039 \\ 0.0229 & 0.0010 & -0.0000 & -0.0001 & -0.9983 & -0.0000 & 0.0536 & 0.0009 & -0.0001 \\ -0.0003 & 0.0007 & 0.8876 & -0.4602 & 0.0000 & 0.0209 & -0.0000 & 0.0000 & -0.0000 \\ 0.0007 & 0.0003 & 0.4601 & 0.8878 & -0.0000 & 0.0093 & 0.0000 & 0.0000 & 0.0000 \\ 0.0000 & -0.0000 & -0.0229 & 0.0014 & 0.0000 & 0.9997 & 0.0000 & 0.0000 & -0.0000 \\ 0.0040 & -0.0081 & 0.0000 & -0.0000 & 0.0000 & 0.0000 & 0.0001 & -0.0429 & 0.4276 \\ -0.0081 & -0.0040 & 0.0000 & 0.0000 & -0.0001 & 0.0000 & 0.0002 & -0.0088 & -0.9039 \\ -0.0041 & -0.0020 & 0.0000 & 0.0000 & -0.0537 & 0.0000 & -0.9984 & -0.0188 & -0.0003 \end{bmatrix} \quad (44)$$

Singular values of 0.00017 and 0.0001 correspond to state x_0 and y_0. It can be inferred from these singular values that x_0 and y_0 are poorly observable, and corresponding columns of **V** reveal the fact that they are very poorly cross co-related observable. So we estimate the principal point offset and focal length in one filter, while attitude and rate bias in the second filter by using the estimates of first filter. From the pinhole camera model, the star vector in the image coordinate system is given by

$$\mathbf{b}_j = \frac{1}{\sqrt{(x_j - x_0)^2 + (y_j - y_0)^2 + f^2}} \begin{bmatrix} -(x_j - x_0) \\ -(y_j - y_0) \\ f \end{bmatrix} \tag{45}$$

Therefore,

$$\frac{\partial \mathbf{b}}{\partial \mathbf{x}} = \begin{bmatrix} \frac{1}{\sqrt{D}} - \frac{(x_j - x_0)^2}{D^{3/2}} & -\frac{(x_j - x_0)(y_j - y_0)}{D^{3/2}} & -\frac{1}{\sqrt{D}}\frac{dx_j}{df} + \frac{(x_j - x_0)\left((x_j - x_0)\frac{dx_j}{df} + (y_j - y_0)\frac{dy_j}{df} + f\right)}{D^{3/2}} \\ -\frac{(x_j - x_0)(y_j - y_0)}{D^{3/2}} & \frac{1}{\sqrt{D}} - \frac{(y_j - y_0)^2}{D^{3/2}} & -\frac{1}{\sqrt{D}}\frac{dy_j}{df} + \frac{(y_j - y_0)\left((x_j - x_0)\frac{dx_j}{df} + (y_j - y_0)\frac{dy_j}{df} + f\right)}{D^{3/2}} \\ \frac{f(x_j - x_0)}{D^{3/2}} & \frac{f(y_j - y_0)}{D^{3/2}} & -\frac{1}{\sqrt{D}} + \frac{f\left((x_j - x_0)\frac{dx_j}{df} + (y_j - y_0)\frac{dy_j}{df} + f\right)}{D^{3/2}} \end{bmatrix} \tag{46}$$

where D is given by

$$D = \sqrt{(x_j - x_0)^2 + (y_j - y_0)^2 + f^2} \tag{47}$$

Simulations

An $8^0 \times 8^0$ field of view star-tracker is simulated by using the pinhole camera model with principal point offsets of x_0=0.75 and y_0=0.25. The focal length of the star camera is assumed to be 64.2964mm. Star tracker data are sampled at 10 Hz and a centroiding noise of mean zero and standard deviation of 17μrad is introduced to the true star data. Plots of the estimated principal point offset, attitude and gyro bias are shown in Figures 12, 13 and 14, respectively. Simulations result show that the algorithm is able to estimate the principal point offset, focal length, attitude and rate bias accurately, but correlation between attitude and principal point offset makes the tuning of the Kalman filter in first approach somewhat difficult. Figures 15, 16 and 17 show the results of the simulation with a centroiding noise standard deviation of 15μrad. It is clear from the results that the attitude estimates are biased. We know that the calibration coefficients are valid when the standard deviation is inline with the projected random error magnitude. So we can perform the covariance consistency test given by equation (42). It is verified that error covariance is again inline with the measurement error covariance. Therefore, it can be concluded that bias in attitude estimation is due to strong correlation between the principal point offset and attitude.

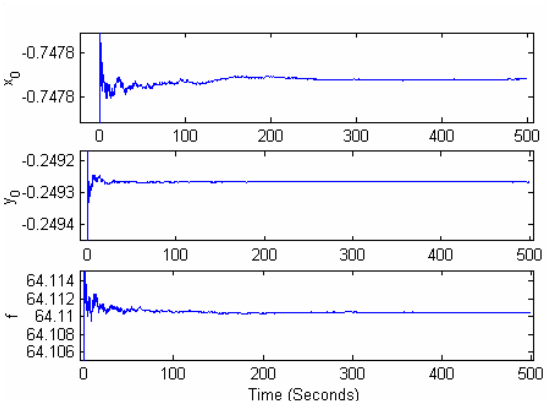

Figure 12: Principal Point offset and Focal Length Estimates ($\sigma_{centrioding\ error}$=17μ rad.)

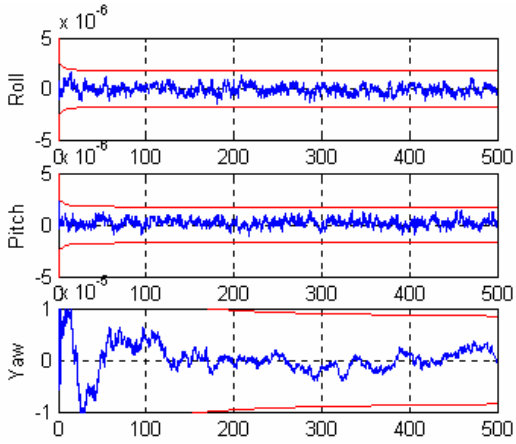

Figure 13: Attitude Estimation Errors ($\sigma_{centrioding\ error}$=17μ rad.)

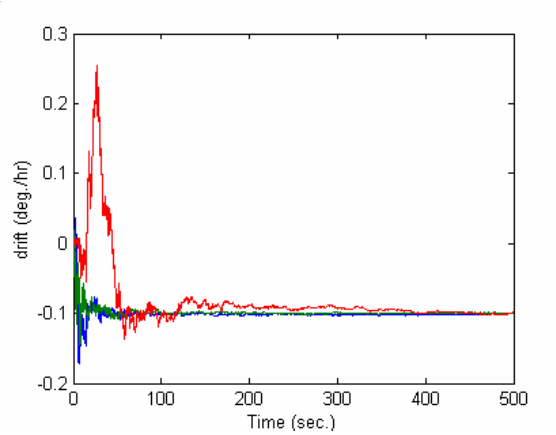

Figure 14: Gyro Bias Estimates
($\sigma_{centrioding\ error}$=17μ rad.)

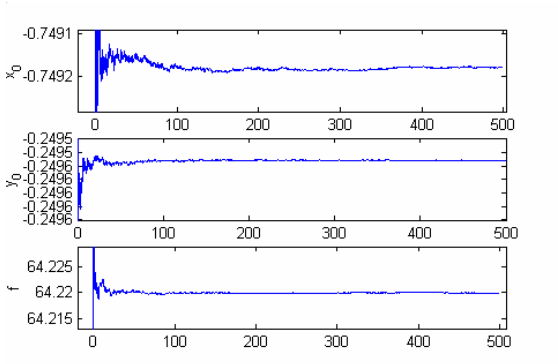

Figure 15: Principal Point offset and focal length estimates ($\sigma_{centrioding\ error}$=15μ rad.)

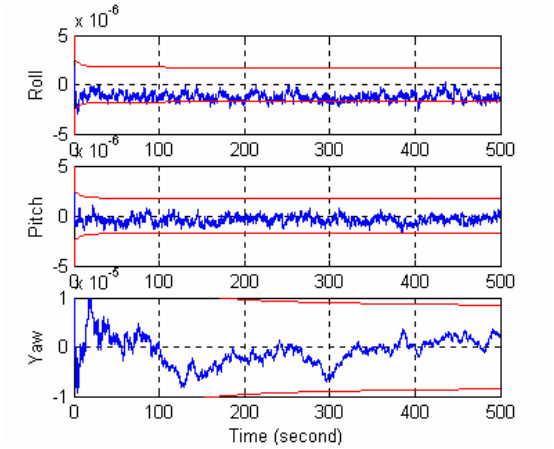

Figure 16: Attitude Estimation Errors
($\sigma_{centrioding\ error}$=15μ rad.)

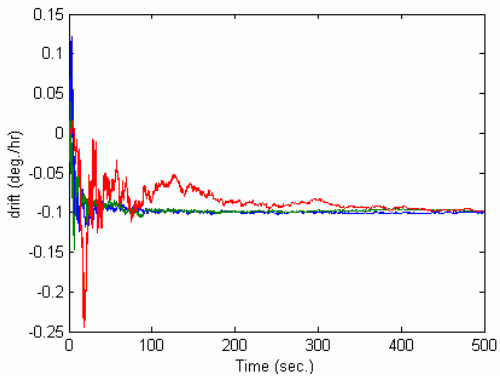

Figure 17: Gyro Bias Estimates
($\sigma_{centrioding\ error}$=15μ rad.)

Attitude Independent Approach

An algorithm has been developed to estimate the principal point offset and focal length without using the attitude information. This approach depends upon the fact that the angle between two vectors is an invariant, whether measured in image frame or inertial frame. Thus we can form the measurement equations that do not depend upon the attitude but do depend upon the uncertain focal length and principal point offset.[16] If these is sufficient information in these measurement equations to estimate the principal point offset and focal length; then we can obtain an accurate attitude. Since the interstar angles for the imaged vectors and the cataloged vectors have to be same, then

$$\cos\left(\theta_{ij}\right) = \mathbf{r}_i^T \mathbf{r}_j = \mathbf{b}_i^T \mathbf{b}_j \tag{48}$$

Now using equation (45) we can show that;

$$\mathbf{r}_i^T \mathbf{r}_j = \frac{N}{D_1 D_2} = g_{ij}\left(x_0, y_0, f\right) \tag{49}$$

where

$$\begin{aligned} N &= \left(x_i - x_0\right)\left(x_j - x_0\right) + \left(y_i - y_0\right)\left(y_j - y_0\right) + f^2 \\ D_1 &= \sqrt{\left(x_i - x_0\right)^2 + \left(y_i - y_0\right)^2 + f^2} \\ D_2 &= \sqrt{\left(x_j - x_0\right)^2 + \left(y_j - y_0\right)^2 + f^2} \end{aligned} \tag{50}$$

Linearization of equation (49) gives

$$R_{ij} = r_i^T r_j - g_{ij}(\hat{x}_0, \hat{y}_0, \hat{f}) = \left[\frac{\partial g_{ij}}{\partial x_0} \quad \frac{\partial g_{ij}}{\partial y_0} \quad \frac{\partial g_{ij}}{\partial f} \right]_{(\hat{x}_0, \hat{y}_0, \hat{f})} \begin{Bmatrix} x_0 \\ y_0 \\ f \end{Bmatrix} \tag{51}$$

$$R_{ij} = [A]\{\Delta Z\}$$

The various derivatives in equation (51) are given by

$$\frac{\partial g_{ij}}{\partial x_0} = \frac{D_1 D_2 (2x_0 - x_i - x_j) + N\left[(x_i - x_0) D_2 / D_1 + (x_j - x_0) D_1 / D_2 \right]}{(D_1 D_2)^2}$$

$$\frac{\partial g_{ij}}{\partial y_0} = \frac{D_1 D_2 (2y_0 - y_i - y_j) + N\left[(y_i - y_0) D_2 / D_1 + (y_j - y_0) D_1 / D_2 \right]}{(D_1 D_2)^2} \tag{52}$$

$$\frac{\partial g_{ij}}{\partial f} = \frac{D_1 D_2 (2f) + Nf\left[D_2 / D_1 + D_1 / D_2 \right]}{(D_1 D_2)^2}$$

By using the EKF, we can show that the solution of equation (51) is given by

$$K_k = P_k A_k^T \left[A_k P_k A_k^T + R_k \right]^{-1}$$

$$\Delta Z_{k+1} = \Delta Z_k + K_k \left[R - g_{ij} \right] \tag{53}$$

$$P_{k+1} = (I - K_k A_k) P_k$$

The above formulation is based upon the assumption that the sensitivity matrix is error free.[13] From equation (51) it is clear that the sensitivity matrix A is still a function of the centroiding coordinates of the stars, which include some random centroiding measurement errors as well as systematic errors that are not known. So the EKF estimates are not guaranteed to be accurate for poor initial guesses. Therefore, a new estimator is developed by the combination of Least Squares (LS) and the Kalman filter. A least squares estimate of the principal point offset is determined from equation (51). Then the LS estimates are used as "measurements" for a recursive Kalman filter to filter out the noise, combining many LS estimates to find a best estimate.

Spacecraft Simulation and Results

A simulation study is performed for the GIFTS mission. The simulated spacecraft is in a geosynchronous orbit. An $8^0 x 8^0$ field of view star camera is simulated by using the pinhole camera model with principal point offsets of x_0=0.75 and y_0=0.25. The focal length of star camera is assumed to be 64.2964mm. Star tracker data are sampled at 10 Hz and a centroiding noise of mean zero and standard deviation of 17μrad is introduced to true star data.

A plot of the LS estimates is shown in figure 18. From this plot, the LS estimates appear to be very noisy. Figure 19 shows the plot of estimated principal point offset and focal length after filtering out the noise from the LS estimates by using a Kalman Filter. The simulation results show that the values of (x_0, y_0) and f converged after 250 seconds. The simulation results also reveal the fact that the focal length convergence is quite robust while x_0 and y_0 are less observable with larger oscillations in their convergence transients. This fact can be supported by the SVD decomposition of matrix A in equation (51). The singular values of the sensitivity matrix give an idea of the degree of observability of the states. Singular values of matrix A are given in Table 1. It is clear from the table that two singular values of matrix A are an

order of magnitude lower than the third one (corresponds to focal length), and therefore principal point offsets are less observable than the focal length. From these figures, it is clear that sequential estimator developed in this paper is able to give accurate estimates of the principal point offset and focal length.

Table 1: Singular Values of A

7.5341e-004	2.1476e-005	1.5472e-005

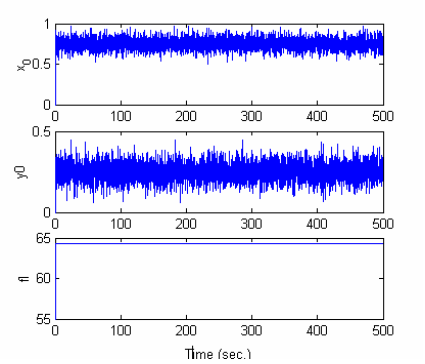

Figure 18: LS Estimate of Boresight Error for Attitude Independent Approach

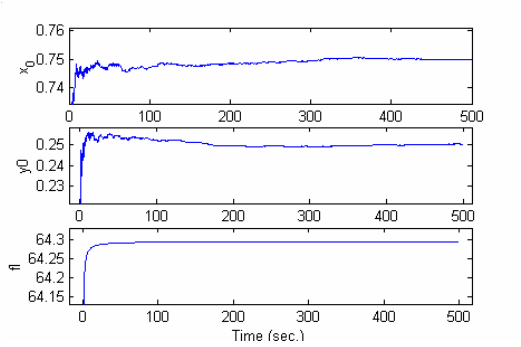

Figure 19: Boresight Error Estimates after Filtering by the Kalman Filter

Variance Analysis

In this section a variance analysis for the attitude independent approach is derived. Consider two body measurements:

$$\begin{aligned} \tilde{\mathbf{b}}_i &= \mathbf{C}(\mathbf{q})\mathbf{r}_i + \mathbf{v}_i \\ \tilde{\mathbf{b}}_i &= \mathbf{C}(\mathbf{q})\mathbf{r}_i + \mathbf{v}_i \end{aligned} \tag{54}$$

where $\mathbf{v_i}$ and $\mathbf{v_j}$ are uncorrelated. Define the following effective measurement

$$\mathbf{z} \equiv \tilde{\mathbf{b}}_i^T \tilde{\mathbf{b}}_j = \mathbf{r}_i^T \mathbf{r}_j + \mathbf{r}_i^T \mathbf{C}^T \mathbf{v}_j + \mathbf{r}_j^T \mathbf{C}^T \mathbf{v}_i + \mathbf{v}_i^T \mathbf{v}_j \tag{55}$$

since $\mathbf{v_i}$ and $\mathbf{v_j}$ are uncorrelated then

$$E\{\mathbf{z}\} = \mathbf{r}_i^T \mathbf{r}_j \tag{56}$$

Define the following variable

$$p \equiv \mathbf{z} - E\{\mathbf{z}\} = \mathbf{r}_i^T \mathbf{C}^T \mathbf{v}_j + \mathbf{r}_j^T \mathbf{C}^T \mathbf{v}_i + \mathbf{v}_i^T \mathbf{v}_j \tag{57}$$

Then taking $E\{p^2\}$ yields

$$\sigma_p^2 = E\{p^2\} = \mathbf{r}_i^T \mathbf{C}^T \mathbf{R}_j \mathbf{C} \mathbf{r}_i + \mathbf{r}_j^T \mathbf{C}^T \mathbf{R}_i \mathbf{C} \mathbf{r}_j + Trace(\mathbf{R}_i \mathbf{R}_j) \tag{58}$$

The last term is typically higher-order, which can effectively be ignored. If $\mathbf{R}_i = \sigma_i^2 \mathbf{I}$ and $\mathbf{R}_j = \sigma_j^2 \mathbf{I}$ then

$$\sigma_p^2 = \sigma_i^2 + \sigma_j^2 + 3\sigma_i^2 \sigma_j^2 \tag{59}$$

Furthermore, if $\sigma_i^2 = \sigma_j^2 = \sigma^2$ then $\sigma_p^2 = 2\sigma^2 + 3\sigma^4$. The residual variance can be computed using the scalar version of the approach given in equation (43). Equation (42) is used to check the consistency of the simulation results. It is found that the left hand-side of this equation matches well with the right hand-side.

Higher Order Focal Plane Calibration

Higher order focal plane distortions can be estimated by making x_0, y_0 and f function of positions, i.e., x_0 and y_0 can be written as

$$\begin{aligned} x_0 &= \mathrm{f}_1(x, y) \\ y_0 &= \mathrm{f}_2(x, y) \end{aligned} \tag{60}$$

As the angle between two vectors is invariant, whether measured in image frame or inertial frame, we can write

$$\begin{aligned} &\mathbf{r}_i^T \mathbf{r}_j = \mathbf{b}_i^T \mathbf{b}_j \\ &\mathbf{b}_i = \frac{1}{D_1}\begin{Bmatrix} -(x_i - x_{0i}) \\ -(y_i - y_{0i}) \\ f \end{Bmatrix}; x_{0i} = \mathbf{\Phi}_i^T \tilde{\mathbf{a}}; y_{0i} = \mathbf{\Phi}_i^T \tilde{\mathbf{b}} \\ &\mathbf{b}_j = \frac{1}{D_2}\begin{Bmatrix} -(x_j - x_{0j}) \\ -(y_j - y_{0j}) \\ f \end{Bmatrix}; x_{oj} = \mathbf{\Phi}_j^T \tilde{\mathbf{a}}; y_{0j} = \mathbf{\Phi}_j^T \tilde{\mathbf{b}} \end{aligned} \tag{61}$$

So, we have

$$\begin{aligned} &\mathbf{r}_i^T \mathbf{r}_j = \frac{N}{D_1 D_2} = g \\ &N = (x_i - x_{0i})(x_j - x_{0j}) + (y_i - y_{oi})(y_j - y_{0j}) + f^2 \\ &D_1 = \left((x_i - x_{0i})^2 + (y_i - y_{oi})^2 + f^2\right) \\ &D_2 = \left((x_j - x_{0j})^2 + (y_j - y_{0j})^2 + f^2\right) \end{aligned} \tag{62}$$

Linearizing equation (62), we obtain

$$\mathbf{r}_i^T \mathbf{r}_j = \frac{\hat{N}}{\hat{D}_1 \hat{D}_2} + \left[\frac{\partial g}{\partial \tilde{\mathbf{a}}} \quad \frac{\partial g}{\partial \tilde{\mathbf{b}}}\right]_{(\hat{\mathbf{a}}, \hat{\mathbf{b}})} \begin{Bmatrix} \tilde{\mathbf{a}} \\ \tilde{\mathbf{b}} \end{Bmatrix} \tag{63}$$

where

$$\frac{\partial g}{\partial \tilde{\mathbf{a}}} = \frac{\partial g}{\partial x_{0i}} \mathbf{\Phi}_i^T + \frac{\partial g}{\partial x_{oj}} \mathbf{\Phi}_j^T, \quad \frac{\partial g}{\partial \tilde{\mathbf{b}}} = \frac{\partial g}{\partial y_{0i}} \mathbf{\Phi}_i^T + \frac{\partial g}{\partial y_{oj}} \mathbf{\Phi}_j^T \tag{64}$$

After computing various partials,

$$\begin{aligned} \frac{\partial g}{\partial x_{0i}} &= \frac{1}{(D_1 D_2)^2}\left[-D_1 D_2 (x_j - x_{0j}) + N \frac{D_2}{D_1}(x_i - x_{0i})\right] \\ \frac{\partial g}{\partial x_{0j}} &= \frac{1}{(D_1 D_2)^2}\left[-D_1 D_2 (x_i - x_{0i}) + N \frac{D_1}{D_2}(x_j - x_{0j})\right] \\ \frac{\partial g}{\partial y_{0i}} &= \frac{1}{(D_1 D_2)^2}\left[-D_1 D_2 (y_j - y_{0j}) + N \frac{D_2}{D_1}(y_i - y_{0i})\right] \\ \frac{\partial g}{\partial y_{0j}} &= \frac{1}{(D_1 D_2)^2}\left[-D_1 D_2 (y_i - y_{0i}) + N \frac{D_1}{D_2}(y_j - y_{0j})\right] \end{aligned} \tag{65}$$

the following equation is given:

$$\mathbf{r}_i^T \mathbf{r}_j - \frac{\hat{N}}{\hat{D}_1 \hat{D}_2} = \begin{bmatrix} \frac{\partial g}{\partial \tilde{\mathbf{a}}} & \frac{\partial g}{\partial \tilde{\mathbf{b}}} \end{bmatrix} \begin{Bmatrix} \tilde{\mathbf{a}} \\ \tilde{\mathbf{b}} \end{Bmatrix} \tag{66}$$

From equation (66) **a** and **b** can be estimated in the same manner as the principal point offset and focal length were estimated. But, selection of the distortion model should be made in a judicious fashion, i.e., various kinds of distortion functions exist in various imagery systems, which take into account the radial and tangential distortions. A good survey of the literature and discussion of methods for CCD cameras calibration is presented by Lenz and Tsai[3]. Tsai method[3] is based upon the assumption that the tangential distortion is negligible as compared to radial distortion. In this paper, we will look for some radial distortion function for lens distortions. The lens distortion is assumed to be given as[2,3]

$$\mathbf{\Phi} = \begin{bmatrix} r & r^2 & r^3 & r^4 \end{bmatrix}^T; \; x_0 = x\mathbf{\Phi}^T\tilde{\mathbf{a}}; \; y_0 = y\mathbf{\Phi}^T\tilde{\mathbf{b}} \tag{67}$$

or

$$\mathbf{\Phi}_x = \begin{bmatrix} x(x^2+y^2) & 3x^2+y^2 & 2xy & x^2+y^2 \end{bmatrix}^T \tag{68}$$

$$\mathbf{\Phi}_y = \begin{bmatrix} y(x^2+y^2) & 3x^2+y^2 & 2xy & x^2+y^2 \end{bmatrix}^T$$

Simulations and Results

A study is performed by simulating an 8^0x8^0 FOV star camera, using the pinhole camera model lens distortion given by equation (61) and (67 & 68). The focal length of star camera is assumed to be 64.2964mm. Star tracker data are sampled at 10 Hz and a centroiding noise of mean zero and standard deviation of 17μrad is introduced to true star data. Figures 20 and 21 show the surface plots of the true distortion functions by using the distortion functions given by equations (67 & 68). Estimated distortion surfaces are shown in figures 22 and 23. The true and estimated values of the distortion parameters are given in Tables 2 and 3. From the results we can conclude that the distortion parameters are successfully estimated by the algorithm developed in this paper, which allows for autonomous calibration of the star camera on-orbit. But in presence of localized distortion, a more judicious selection of the distortion parameters is needed.

Table 2: True and Estimated Distortion Parameters for Distortion Given by Equation (67)

a_{true}	a_{est}	b_{true}	b_{est}
5e-04	-5.1127e-004	8e-04	-8.2594e-004
2e-04	-1.9572e-004	-5e-04	5.0775e-004
-3.4e-04	3.5959e-004	5.6e-04	-5.7828e-004
-5.3e-04	5.3435e-004	-3.4e-04	3.8590e-004

Table 3: True and Estimated Distortion Parameters for Distortion Given by Equation (68)

a_{true}	a_{est}	b_{true}	b_{est}
5e-04	-4.5920e-004	8e-04	-9.2657e-004
2e-04	-2.4988e-004	-5e-04	5.6702e-004
-3.4e-05	5.1022e-005	5.6e-05	-6.9582e-005
-5.3e-06	3.5486e-006	-3.4e-06	4.2967e-006

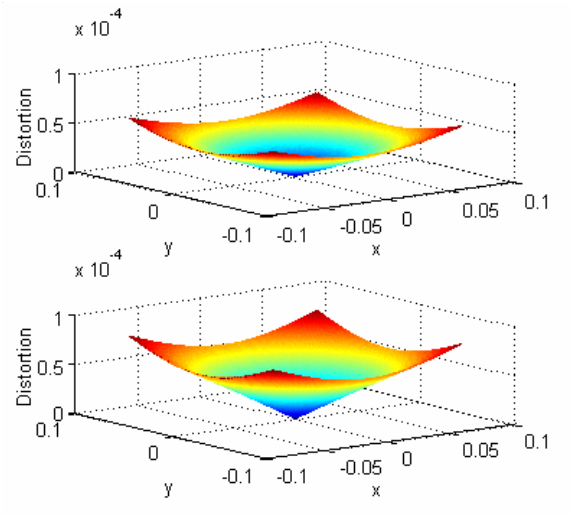

Figure 20: True Distortion Surface for Distortion Basis Function Given by Equation (67)

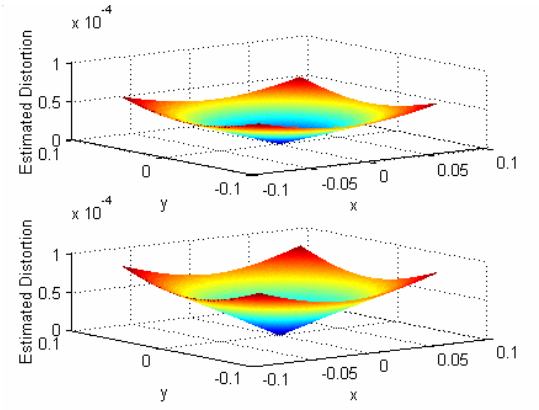

Figure 21: Estimated Distortion Surface for Distortion Basis Function Given by Equation (67)

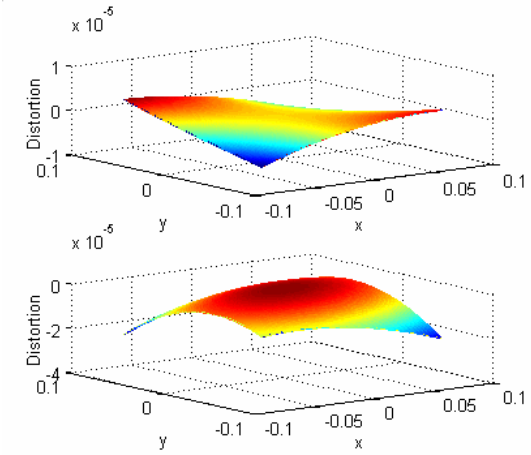

Figure 22: True Distortion Surface for Distortion Basis function Given by Equation (68)

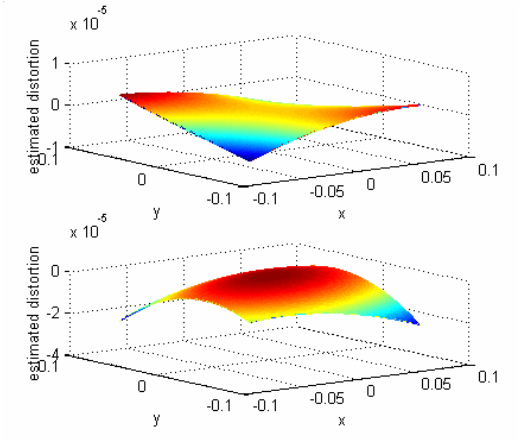

Figure 23: Estimated Distortion Surface for Distortion Basis Function Given by Equation (68)

Conclusions

The Kalman filter algorithm was developed in this paper for attitude, interlock angle and rate bias determination using three-axis gyro data and split field of view star camera measurements. Two algorithms were presented for focal plane distortion estimation. In the attitude dependent approach, focal plane distortion estimation depends upon the estimated attitude and vice-versa. The strong coupling between principal point offset and attitude makes this algorithm numerically unstable. A novel approach was developed for the focal plane calibration using the measurements independent of attitude. The results indicated the algorithms developed in this paper provide precise estimates of attitude, interlock angle, principal point offset, focal length, and higher order focal plane distortion and gyro rate bias.

Acknowledgements

We are pleased to acknowledge Dr. T.C. Pollock (Associate Professor, Aerospace Engineering Department, Texas A&M University) for the creation of the split field of view star camera.

References

1. Sidi J.M., "Spacecraft Dynamics and Control," Cambridge University Press 1997.
2. Guoqing Z., Tang X., Baozong Y., "Distortion Model Selecting and Accuracy Evaluation for CCD Camera Calibration," *Proceedings of ICSP' 96*.
3. Lenz K.R., Tsai Y.R., "Techniques for Calibration of the scale factor and Image Center for High Accuracy 3-D Machine Vision Metrology," *IEEE Transactions on Pattern Analysis and Machine Intelligence*, Vol. 10, No. 5, September 1988, pp 713-720.
4. Crassidis, J.L., and Markley, F.L., "State Estimation Techniques," book chapter in *Spacecraft Orbit and Attitude Systems*, edited by J.R. Wertz, in progress.
5. Crassidis, J.L., and Junkins, J.L., "An Introduction to Optimal Estimation of Dynamical Systems," second edition, in progress.
6. Junkins J.L., " Optimal Estimation of Dynamical Systems," Sijthoff and Noordhoff International Publishers B.V., Alphan aan den Rijn, The Netherlands, 1978.
7. Junkins J.L. and Kim, Y., "Introduction to Dynamics and Control of Flexible Structures," *AIAA Education Series*, Reston, VA, 1993.
8. Zarchan P., Musoff H., " Fundamentals of Kalman Filtering: A Practical Approach," Volume 190, *Progress in Astronautical and Aeronautics*, AIAA Education Series, Reston, VA, 2000.
9. Hamilton, W.R., "Elements of Quaternion," London: Longmans, Green.
10. Lefferts E.J., Markley F.L. and Shuster M.D., "Kalman Filtering For Spacecraft Attitude Estimation," *Journal of Guidance, Control and Dynamics*, Vol: 5, No. 5, Sept.-Oct. 1982, pp 417-429.
11. Farrenkopf R.L., "Analytical Steady-State Accuracy Solution for Two Common Spacecraft Estimators," *Journal of Guidance, Control and Dynamics*, Vol. 1, No. 4, pp 282-283.
12. Mortari D., Junkins J.L. and Samaan M.A., " Lost-In-Space Pyramid Algorithm for Robust Star Pattern Recognition," *Paper AAS 01-004 Guidance and Control Conference*, Breckenridge, Colorado, 31 Jan.-4 Feb. 2001.
13. Samaan M.A., Mortari D. and Junkins J.L., "Recursive Mode Star Identification Algorithms," *Paper AAS 01-149 AAS/AIAA Space Flight Mechanics Meeting*, Santa Barbara, California, 11 Jan.- 15 Feb. 2001.
14. Wahba G., "A Least Square Estimate of Satellite Attitude," Problem 65-1, SIAM *Review*, Vol. 7, No. 3, July 1965, pg. 409.
15. Griffith D.T., Singla P., and Junkins J.L., "Autonomous On-Orbit Calibration Approaches For Star-Tracker Cameras", *AAS/AIAA Space Flight Mechanics Meeting*, San Antonio, TX, USA, 27-30 January, 2002, Paper AAS 02-102.
16. Samaan M.A., Griffith T., Singla P. and Junkins J.L., "Autonomous On-orbit Calibration of Star Trackers," *2001 Core Technologies For Space Systems Conference*, Nov. 28-30 2001, Colorado.